

## PAPER

# Medical Image Segmentation Using Level Set Method with a New Hybrid Speed Function Based on Boundary and Region Segmentation

Jonghyun PARK<sup>†a)</sup>, Soonyoung PARK<sup>†</sup>, *Members*, and Wanhyun CHO<sup>††</sup>, *Nonmember*

**SUMMARY** This paper presents a new hybrid speed function needed to perform image segmentation within the level-set framework. The proposed speed function uses both the boundary and region information of objects to achieve robust and accurate segmentation results. This speed function provides a general form that incorporates the robust alignment term as a part of the driving force for the proper edge direction of an active contour, an active region term derived from the region partition scheme, and the smoothing term for regularization. First, we use an external force for active contours as the Gradient Vector Flow field. This is computed as the diffusion of gradient vectors of a gray level edge map derived from an image. Second, we partition the image domain by progressively fitting statistical models to the intensity of each region. Here we adopt two Gaussian distributions to model the intensity distribution of the inside and outside of the evolving curve partitioning the image domain. Third, we use the active contour model that has the computation of geodesics or minimal distance curves, which allows stable boundary detection when the model's gradients suffer from large variations including gaps or noise. Finally, we test the accuracy and robustness of the proposed method for various medical images. Experimental results show that our method can properly segment low contrast, complex images.

**key words:** *image segmentation, geometric deformable model, level set method, gradient vector flow*

## 1. Introduction

Medical image processing has revolutionized the field of medicine by providing novel methods to extract and visualize medical data information acquired through various acquisition modalities. Image segmentation is one of the most important steps in the analysis of preprocessed patient image data and can be helpful in diagnosis, treatment planning, and treatment delivery, among other applications [1]–[3]. It is the process of labeling each pixel in a medical image dataset to indicate its tissue type or anatomical structure. The accurate estimation of tumor size is important for clinical reasons, e.g., for treatment planning and therapy evaluation. Although maximum tumor diameter is widely used as an indication of tumor size, it may not reflect a proper assessment of this tumor attribute because of the tumor image nature and irregular shape of the tumor. One way to obtain an estimate of tumor volume is via segmentation. Since the former approach using tumor volume generally achieves higher accuracy, it is the main focus of our research. There

are several proposed approaches in the literature for image segmentation and extraction of objects (tumor, vessel, bone, etc.).

Segmentation techniques can be categorized into four classes: the threshold-based, edge or boundary-based, region-based and model-based techniques [1], [4]–[6]. The threshold technique is the most intuitive. This technique is based on local pixel intensity levels. The current image is compared to the background image, and a threshold value decides if the pixel differs enough to belong to the foreground. Clearly, additional filtering and clustering have to be considered because the background can also vary according to possible noise. The edge-based technique is by far the most common method of detecting boundaries and discontinuities in an image. An edge is a set of connected pixels with the same intensity level between two adjacent pixels and can be distinguished by estimating the intensity gradient. The region-based technique partitions an image into regions. First, the image is searched for boundaries and discontinuities in areas where there are large intensity changes in the pixel values. A region is formed by a closed path. Then some kind of region growing is applied by inducing the merger of smaller regions with larger regions. This procedure results in well-separated regions that are defined by the intensity level difference. The model-based technique labels pixels according to probability values, which are determined based on the intensity distribution of an image. Given only the intensity distribution of an image, statistical approaches attempt to estimate the associated class label by making an assumption about the distribution.

In this paper, we are mainly interested in the image segmentation method using the active contour model. This is usually based on minimizing functionals, which would result in small values for curves close to target boundaries. To solve these functional minimization problems, a corresponding partial differential equation is constructed as the gradient decent flow resulting in curve evolution. Moreover, we convert this task within the level-set framework and propose a new hybrid speed function using the level-set method for image segmentation. Our hybrid speed function uses both the boundary and region information of objects to achieve robust and accurate segmentation results. The hybrid speed function reflects a general form that incorporates the robust alignment term, the geodesic active contour model for regularization and the region partition scheme.

Manuscript received October 20, 2011.

Manuscript revised March 23, 2012.

<sup>†</sup>The authors are with Mokpo National University, Korea.

<sup>††</sup>The author is with Chonnam National University, Korea.

a) E-mail: pjhyun@mokpo.ac.kr

DOI: 10.1587/transinf.E95.D.2133

First, although the image gradient aligns appropriately to detect the local edge direction of the precise boundary of the target object, the speed function based image gradient shows dependency on initialization and a poor convergence to boundary concavities. In regard with these weak points, we will use an external force for active contours as gradient vector flow (GVF). GVF is computed as the diffusion of gradient vectors of a gray-level edge map derived from the target image. Second, although active contour models based on object boundary are used extensively in image segmentation, they tend to be slower and prone to the leakage of contours outside the object boundary in images with intensity inhomogeneity. However, this limitation can be overcome by a region-based segmentation method that separates an object from the background in an image. This method partitions the image domain by progressively fitting statistical models to the intensity in each region. This paper adopts two Gaussian distributions to model the intensity distribution of the inside and outside of the evolving curve partitioning the image domain. Third, we use an active contour model that has the computation of geodesics or minimal distance curves, which allows stable boundary detection when the model's gradients suffer from large variations, including gaps.

Finally, we conduct a test to determine the accuracy and robustness of the proposed method for various synthetic and medical images. The rest of this paper proceeds as follows: Sect. 2 provides a brief literature review. Section 3 presents the proposed method. Section 4 evaluates the viability of the method for low-contrast, complex-image segmentation, provides the results, and concludes.

## 2. Review of the Deformable Model

### 2.1 Geometric Integral Measures for Active Contours

Let us consider a gray level image as a function  $I: \Omega \rightarrow \mathfrak{R}^+$ , where  $\Omega \subseteq \mathfrak{R}^2$  is the image domain. We search for the contour  $C: [0, L] \rightarrow \mathfrak{R}^2$ , given in a parametric form by the arc length  $s$  as  $C(s) = \{(x(s), y(s)) : 0 \leq s \leq L\}$ . Given the curve  $C$ , we denote the inside and outside of the curve as  $\Omega_c$  and  $\Omega \setminus \Omega_c$ , respectively. The energy functional  $E(C)$  for a contour  $C$  can be defined as two types of integral measures that are related via the Green theorem [7], [8]. The first functional integrates the function  $L(C_s, C)$  defined on the curve and is considered as a boundary-based measure in the general form of:

$$E_1(C) = \int_0^L L(C_s, C) ds. \quad (1)$$

$$L(C_s, C) = \{(x(C_s, C), y(C_s, C)) : 0 \leq C_s \leq L, 0 \leq C \leq L\}$$

The second functional integrates the values of the function  $f(x, y)$  inside the curve and is usually referred to as a region based measure:

$$E_2(C) = \iint_{\Omega_c} f(x, y) dx dy. \quad (2)$$

Formally, we search for the optimal planar curve  $C$  such that

$$C = \arg \min_C E(C) \quad \text{or} \quad C = \arg \max_C E(C). \quad (3)$$

Here, by using the calculus of variations for the two functionals, the curve that minimizes (or maximizes) these functionals can be identified by a differential equation known as the Euler-Lagrange Equation:

$$\frac{\delta E(C)}{\delta C} = \begin{cases} \frac{\partial L}{\partial x} - \frac{\partial}{\partial s} \frac{\partial L}{\partial x_s} = 0 \\ \frac{\partial L}{\partial y} - \frac{\partial}{\partial s} \frac{\partial L}{\partial y_s} = 0 \end{cases}. \quad (4)$$

A dynamic process known as gradient descent, which takes an arbitrary curve toward a minimum (or maximum) of  $E(C)$ , is given by the curve evolution equation

$$\frac{\partial C}{\partial t} = -\frac{\delta E(C)}{\delta C}. \quad (5)$$

The virtual time parameter  $t$  is added to our curve to allow its evolution into a family of planar curves  $C(s, t)$ . The key idea is to evolve the boundary  $C$  from some initialization in direction of the negative energy gradient, which can be done by implementing the gradient descent equation:

$$\frac{\partial C}{\partial t} = -\frac{\delta E(C)}{\delta C} = F \cdot \vec{N}, \quad (6)$$

which models an evolutionary path along the normal  $\vec{N}$  with the speed function  $F$ .

### 2.2 Snakes

The traditional snake model [9] is a curve  $C(s)$ ,  $s \in [0, 1]$ , that moves through the spatial domain of an image to minimize the energy functional

$$E(C) = E_{\text{int}} + E_{\text{ext}}, \quad (7)$$

where  $E_{\text{int}}$  and  $E_{\text{ext}}$  denote the internal and external energies, respectively. The internal energy function determines the regularity of a contour. A common choice for internal energy is a quadratic function given by

$$E_{\text{int}} = \int_0^1 (\alpha |C'(s)|^2 + \beta |C''(s)|^2) ds, \quad (8)$$

where  $\alpha$  and  $\beta$  are weighting parameters that control the snake's tension and rigidity. The external energy term that determines the criteria of contour evolution depending on the image  $I(x, y)$  can be defined as

$$E_{\text{ext}} = \int_0^1 g(|\nabla I(C(s))|) ds. \quad (9)$$

A common example of the edge attraction function is a reciprocal of the image gradient given by

$$g(|\nabla I(C(s))|) = \frac{1}{1 + \lambda |\nabla G_{\sigma} * I(x, y)|} \quad (10)$$

where  $G$  denotes a Gaussian smoothing filter with the standard deviation  $\sigma$ ,  $\lambda$  is the suitable constant chosen, and  $*$  is the convolution operator. Solving the problem of snakes involves the identification of a contour  $C$  that minimizes the total energy term  $E(C)$ . It must satisfy the Euler equation

$$\alpha C''(s) + \beta C''''(s) - \nabla E_{\text{ext}} = 0. \tag{11}$$

A numerical solution to this equation can be found by using a greedy algorithm with a given set of weights  $\alpha$  and  $\beta$ .

### 2.3 Geodesic Active Contours

The geodesic active contour model [10], [11] can be considered a particular class of snake models, where the rigidity coefficient is set to zero, i.e.,  $\beta = 0$ . Then the energy functional of this model is defined as

$$E(C) = \int_0^1 g(|\nabla I(C(s))|) |C'(s)| ds. \tag{12}$$

Thus, when trying to detect an object, we are interested in finding not only the path of minimal classical length but also the one that minimizes a new length definition that takes into account image characteristics. In order to minimize this functional, we search for its gradient decent direction. Thus, according to the steepest decent method, we follow the curve evolution equation

$$\frac{\partial C(t)}{\partial t} = \nabla g \kappa \vec{N} - \langle \nabla g, \vec{N} \rangle \vec{N}, \tag{13}$$

where  $\kappa$  is the Euclidean curvature,  $\vec{N}$  is the unit inward normal, and the right-hand side of the equation is given by the Euler-Lagrange formula.

### 2.4 Chan-Vese Minimal Variance Model

In general, a common problem with boundary-based active contour models is that if the target boundary is not well-defined or contains weak parts, the active contour can easily leak through the target boundary and it converges to the wrong solution. To overcome the leakage problem, Chan-Vese suggested the use of the region information of the target object for segmentation [12], [13]. They proposed to minimize the following energy function with respect to  $c_1$ ,  $c_2$ , and  $C$ :

$$E(c_1, c_2, C) = \iint_{\Omega_c} (I - c_1)^2 dx dy + \iint_{\Omega \setminus \Omega_c} (I - c_2)^2 dx dy + \nu |C|. \tag{14}$$

The first two terms in the above functional measure the variations inside and outside the active contour, respectively, whereas the third term measures the length of the contour. The associated curve evolution equation is given by

$$\frac{\partial C(t)}{\partial t} = (c_2 - c_1) \left( I - \frac{c_1 + c_2}{2} \right) \vec{N}, \tag{15}$$

$$c_1 = \frac{1}{|\Omega_c|} \iint_{\Omega_c} I dx dy, \quad c_2 = \frac{1}{|\Omega \setminus \Omega_c|} \iint_{\Omega \setminus \Omega_c} I dx dy.$$

## 2.5 Geodesic Active Region Model

Although initially introduced for supervised texture segmentation, the geodesic active region model has been extended to address unsupervised image segmentation [13], [14]. It has also been successfully exploited to provide an elegant solution to motion estimation and the tracking problem. Then the energy functional of this model is defined as

$$E(C) = \alpha \left( \iint_{\Omega_c} \log(p_1(I(w))) dw + \iint_{\Omega \setminus \Omega_c} \log(p_2(I(w))) dw \right) + (1 - \alpha) \int_0^1 g(|\nabla I(C(s))|) |C'(s)| ds, \tag{16}$$

where  $p_1(I(w))$  and  $p_2(I(w))$  denote the probability density functions of image intensities for the regions  $\Omega_c$  and  $\Omega \setminus \Omega_c$ .

The object functional is minimized by using a gradient descent method. If we compute Euler-Lagrange equations using the Stokes theorem, then we should deform the curve  $C$  by using the following equation:

$$\frac{\partial C(t)}{\partial t} = \alpha (\log(p_1(I(w))) - \log(p_2(I(w)))) \vec{N} + (1 - \alpha) (g(I) \kappa \vec{N} - \langle \nabla g, \vec{N} \rangle \vec{N}). \tag{17}$$

The obtained partial differential equation (PDE) motion equation has two types of forces (i.e., the region force and the boundary force) acting on the propagating curve in the direction of the normal.

## 3. A New Hybrid Level Set Method

### 3.1 Level Set Method

In general, one can distinguish between explicit (parametric) and implicit representations of contours. In explicit representations, a contour is defined as a mapping from an interval to the image domain:  $C: [0, 1] \rightarrow \Omega$ . The propagation of an explicit contour is typically implemented by a set of ordinary differential equations acting on the control or marker points [23], [24]. In implicit contour representations, contours are represented as the level set of the scalar embedding function  $\phi: \Omega \rightarrow \mathfrak{R}$  defined in the image plane. A contour is defined as the zero level set of  $\phi$  such that

$$\phi(\omega) = \begin{cases} \phi(\omega) > 0 & \text{on } \omega \in \Omega_c \\ \phi(\omega) = 0 & \text{on } \omega \in C \\ \phi(\omega) < 0 & \text{on } \omega \in \Omega / \Omega_c \end{cases}. \tag{18}$$

We illustrate the above assumptions and notations on the level set function  $\phi$ , defining the evolving curve  $C$  in Fig. 1. For more details, we refer the reader to [15].

There are various methods to evolve implicitly represented contours. The most popular among these is the level

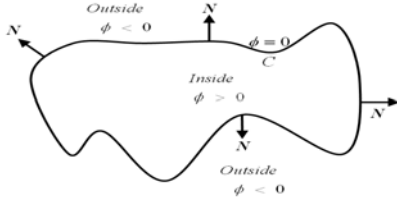


**Fig. 1** Curve  $C = \{(x, y) : \phi(x, y) = 0\}$  propagating in normal direction.

set method, in which a contour is propagated by evolving a time-dependent embedding function  $\phi(\omega, t)$  according to an appropriate PDE [15]. For a contour that evolves along the normal  $\vec{N}$  with a speed  $F$ , one can drive a corresponding partial differential equation for the embedding function  $\phi$  as follows. Because the function  $\phi$  takes zero value on the contour of the curve at all times, the total time derivative of  $\phi$  at boundary point of the contour must vanish:

$$\frac{d\phi(C(t), t)}{dt} = \nabla\phi \frac{\partial C}{\partial t} + \frac{\partial\phi}{\partial t} = \nabla\phi F \cdot \vec{N} + \frac{\partial\phi}{\partial t} = 0. \quad (19)$$

Inserting the definition of the normal  $\vec{N} = \frac{\nabla\phi}{|\nabla\phi|}$ , we get the evolution equation for  $\phi$ :

$$\phi_t = \frac{\partial\phi}{\partial t} = |\nabla\phi| \cdot F. \quad (20)$$

By derivation, this equation only specifies the evolution of  $\phi$  and the values of the speed function  $F$  at the location of the contour. Because the level set function  $\phi$  increases from its initial stage, the corresponding set of contours  $C$  propagate toward outside. In addition, because the evolution of a contour is equivalent to the evolution of the level set function, a contour can be defined as the border between positive and negative areas of the level set function. Thus, contours can be identified by just checking the sign of  $\phi$ . Furthermore, the initial level set function  $\phi_0$  may be provided by the signed distance from the initial contour:

$$\phi_0(\omega) = \pm D(\omega, N_\omega(C_0)), \quad (21)$$

where  $\pm D(a, b)$  denotes a signed distance between  $a$  and  $b$  and  $N_\omega(C_0)$  denotes the nearest neighboring pixel on initial contours  $C_0$ . The initial level set function  $\phi_0$  is zero at the initial contour points of  $C_0$ .

### 3.2 Speed Function Induced from the Robust Alignment of Objects

First, we consider the active contour model with the speed function derived from the boundary information of an object. In many cases, gradient information is used as the stopping criteria for active curve evolution as well as the attracting force to the zero level set from a target boundary. The reason is that the image gradient direction is a good estimator of the orientation of the edge contour. However, for images with intensity inhomogeneity, gradients based these properties can never fully stop the level set evolution even for idea edges, making leakage often inevitable. Hence, we

explore a new edge indicator vector embedded with a speed term.

An ideal selection is to choose an edge indicator vector as the gradient vector flow (GVF) field proposed in Xu and Prince [16]. Then particular advantages of this field are its insensitivity to initialization and its ability to move into boundary concavities. To obtain the GVF field, we first define an edge map  $f(x, y)$  derived from the image  $I(x, y)$  having a property such that it is larger near the image edges. We next define the GVF field to be a vector field  $V_{GVF}(x, y)$  that minimizes the energy functional:

$$E(V_{GVF}) = \int_{\mathbb{R}^2} \mu |\nabla V(x, y)|^2 + |\nabla f|^2 |V(x, y) - \nabla f|^2 dx dy. \quad (22)$$

Using the calculus of variations, we find that the GVF field must satisfy the Euler equation

$$\mu \nabla^2 V - |\nabla f|^2 (V - \nabla f) = 0, \quad (23)$$

where  $\nabla^2$  is applied to each component of the vector field  $V(x, y)$  separately.

Finally, if we replace the image gradient vector field with the GVF field by using a robust alignment measure defined as the absolute value of the inner product between the vector field and the curve normal, we obtain the following functional:

$$E_A(C) = \oint_C |\langle V_{GVF}, \vec{N} \rangle| ds. \quad (24)$$

By the variational principle, the extremals of this functional  $E_A(C)$  can be identified by the Euler Lagrange equation, which is given by the curve evolution equation:

$$\frac{\partial C}{\partial t} = \text{sign}(\langle V_{GVF}, \vec{N} \rangle) \text{div}(V_{GVF}) \vec{N}. \quad (25)$$

Thus, the corresponding curve evolution equation of the level-set formulation is given by

$$\phi_t = \frac{\partial\phi}{\partial t} = \text{sign}(\langle V_{GVF}, \nabla\phi \rangle) \text{div}(V_{GVF}) |\nabla\phi|. \quad (26)$$

Hence, we have the new speed function, which is defined as  $F = \text{sign}(\langle V_{GVF}, \nabla\phi \rangle) \text{div}(V_{GVF})$ .

### 3.3 Speed Function Induced from the Active Region of Objects

Second, let us consider the geometric active contour model, which uses the region information of target objects for segmentation. This model can not only solve some weak points in the boundary based model, such as the dependency of local information and initialization, but also optimally partition a given image as some homogenous regions.

First, we assume that a regular curve  $C$  splits an image domain  $\Omega$  as disjoint regions  $\Omega_1$  and  $\Omega_2$ . We also assume that all partitions are equally possible

$$p(I | \{\Omega_1, \Omega_2\}) = p(I | \Omega_1) p(I | \Omega_2) \quad (27)$$

and that the pixels within each regions are independent

$$p(I | \Omega_i) = \prod_{w \in \Omega_i} p(I(w)), \quad i = 1, 2. \quad (28)$$

Then the joint probability of intensity values  $I$  observed at a given image partition  $\Omega = \{\Omega_1, \Omega_2\}$  is given by

$$p(I | \{\Omega_1, \Omega_2\}) = p(I | \Omega_1)p(I | \Omega_2) = \prod_{w \in \Omega_1} p_1(I(w)) \prod_{w \in \Omega_2} p_2(I(w)). \quad (29)$$

Here the optimal segmentation is found by minimizing the following energy functional:

$$E(\Omega_1, \Omega_2) = - \left( \int_{\Omega_1} (\log p_1(I(w))) dw + \int_{\Omega_2} (\log p_2(I(w))) dw \right). \quad (30)$$

Here, by using the Heaviside function  $H$  and the one-dimensional Dirac measure  $\delta$  concentrated at zero defined respectively by

$$H(z) = \begin{cases} 1 & \text{if } z \geq 0 \\ 0 & \text{if } z < 0 \end{cases} \quad (31)$$

and

$$\delta(z) = \frac{d}{dz} H(z), \quad (32)$$

we can express the above energy functional as the following level-set form:

$$E(\phi) = - \left( \int_{\Omega} H(\phi(w)) \log p_1(I(w)) dw + \int_{\Omega} (1 - H(\phi(w))) \log p_2(I(w)) dw \right). \quad (33)$$

Then the corresponding Euler-Lagrange evolution equation for  $\phi$  is given by

$$\frac{\partial \phi}{\partial t} = \delta(\phi(w)) (\log p_1(I(w)) - \log p_2(I(w))). \quad (34)$$

A standard rescaling can be made by replacing  $\delta(\phi)$  by  $|\nabla \phi|$  and this then gives the following equation:

$$\phi_t = |\nabla \phi(w)| (\log p_1(I(w)) - \log p_2(I(w))). \quad (35)$$

Here we have assumed that the probability distribution of intensity values is generally modeled by the Gaussian distribution. Thus, probability distributions of pixel values in each region  $\Omega_i$  are given by

$$p_1(I(w)) = \varphi(I(w); \mu_1, \sigma_1^2), \quad \varphi(I(w); \mu_1, \sigma_1^2) = (2\pi\sigma_1^2)^{-1/2} \exp\left(-\frac{1}{2\sigma_1^2}(I - \mu_1)^2\right) \quad (36)$$

and

$$p_2(I(w)) = \varphi(I(w); \mu_2, \sigma_2^2), \quad \varphi(I(w); \mu_2, \sigma_2^2) = (2\pi\sigma_2^2)^{-1/2} \exp\left(-\frac{1}{2\sigma_2^2}(I - \mu_2)^2\right), \quad (37)$$

where  $\mu_k$  and  $\sigma_k^2$  are the mean and variance of each Gaussian distribution, respectively. First, the parameters  $\{\mu_k, \sigma_k^2, k = 1, 2\}$  in the Gaussian probability distribution of each region can be estimated by applying the Maximum likelihood method as follows:

$$\hat{\mu}_k = \frac{1}{|\Omega_k|} \sum_{w \in \Omega_k} I(w), \quad \hat{\sigma}_k^2 = \frac{1}{|\Omega_k| - 1} \sum_{w \in \Omega_k} (I(w) - \hat{\mu}_k)^2, \quad k = 1, 2. \quad (38)$$

### 3.4 New Hybrid Speed Function for Deformable Model

Numerous active contour models have been developed as paradigms for boundary-based and region-based methods [17]–[19]. Here we have considered a novel segmentation method using level set evolution by introducing a new speed term. This is given as a weighted sum of three types of measures, i.e., a robust alignment term, an active region term, and a smoothing term derived from different geometric functional, and is represented as follows:

$$F = \alpha(\text{sign}(\langle V_{GVF}, \nabla \phi \rangle)) \text{div}(V_{GVF}) + \beta(\log p_1(I(w)) - \log p_2(I(w))) + \gamma \left( g(I) \text{div} \left( \frac{\nabla \phi}{|\nabla \phi|} \right) - \left\langle \nabla g, \frac{\nabla \phi}{|\nabla \phi|} \right\rangle \right) \quad (39)$$

Thus, the corresponding level set equation of curve evolution is given by

$$\phi_t = F|\nabla \phi| \quad \text{or} \quad \phi^{(t)} = \phi^{(t-1)} + \Delta t F|\nabla \phi|. \quad (40)$$

## 4. Experimental Results

This section presents segmentation results using level-set approach with a new hybrid speed function based boundary and region information on various synthetic, medical and real images, with different types of contours, intensities, texture and shapes.

### 4.1 Property Analysis of Parameter Values

We show that three parameters of the proposed algorithm do not depend on the initial value based on various initial values. Therefore, we test the proposed algorithm to the synthetic image to analyze the segmentation performance by adjusting the parameters. First, in Fig. 2, we show how our model works on a blurred synthetic image, with various shapes and an interior contour, which is automatically detected. Due to the level set implementation, the model allows automatically change of topology. In Fig. 3, we show that our model can detect different objects of noisy synthetic

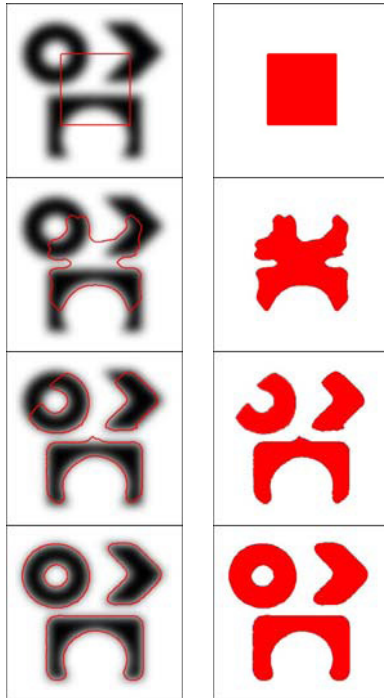


**Fig. 2** Detection of three blurred objects of distinct shapes ( $\alpha = 0.2$ ,  $\beta = 0.6$ ,  $\gamma = 0.2$ ).

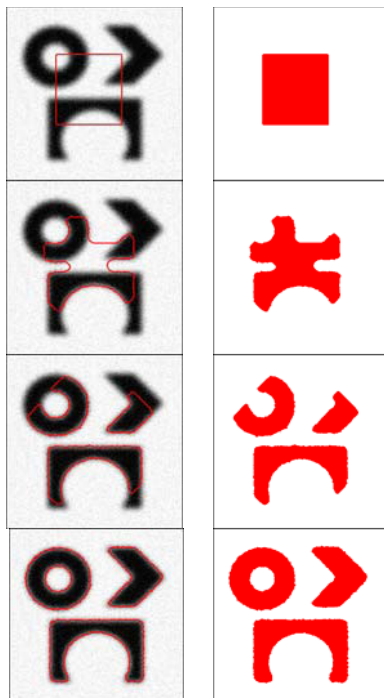


**Fig. 3** Detection of three blurred objects with noise of distinct shapes ( $\alpha = 0.2$ ,  $\beta = 0.3$ ,  $\gamma = 0.5$ ).

image with blurred boundaries. The curve is also automatically attracted toward the objects. As expected, we can observe that the active region term and smoothing term have a dominant role in the segmentation for the blurred and noisy images. And the robust alignment term leads the active con-

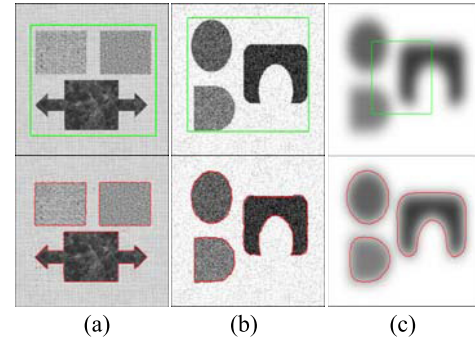


**Fig. 4** Results of segmentation by  $\alpha$ ,  $\beta$  and  $\gamma$  parameter values of the proposed speed function. (a) texture image ( $\alpha = 0.6$ ,  $\beta = 0.1$ ,  $\gamma = 0.3$ ), (b) noisy image ( $\alpha = 0.2$ ,  $\beta = 0.3$ ,  $\gamma = 0.5$ ), and (c) blurred image ( $\alpha = 0.1$ ,  $\beta = 0.6$ ,  $\gamma = 0.3$ ).

**Table 1** ACC value using three parameters for texture image.

$\beta \backslash \alpha$	0.1	0.2	0.3	0.4	0.5	0.6	0.7	0.8
0.1				0.968	0.969	0.969	0.971	0.966
0.2			0.976	0.974	0.974	0.975	0.966	
0.3		0.978	0.975	0.974	0.973	0.966		
0.4	0.976	0.977	0.97	0.967	0.963			$\gamma=0.1$
0.5	0.963	0.974	0.967	0.958				$\gamma=0.2$
0.6	0.964	0.967	0.958					$\gamma=0.3$
0.7	0.958	0.959						$\gamma=0.4$
0.8	0.958							$\gamma=0.5$

tour to the accurate edge locations in the object region.

To assess the segmentation performance by  $\alpha$  (robust alignment term),  $\beta$  (active region term), and  $\gamma$  (smoothing term) parameter values of the hybrid speed function for various images, we apply the level set procedure for the texture, noise and blurred images, respectively, in Fig. 4 (a). The second row is results of segmentation using  $\alpha$ ,  $\beta$  and  $\gamma$  parameter values of the proposed speed function. The three terms of the proposed speed function are required to be weighted properly to guide the evolving curve under different image conditions. We have used the measure proposed by [26], to numerically evaluate the segmentation results obtained using various of the parameters. The overall accuracy (ACC) of the segmentation result can be estimated using the following equation;

$$ACC = \frac{TP + TN}{TP + TN + FP + FN} \tag{41}$$

where  $TP$ ,  $TN$ ,  $FP$ ,  $FN$  are true positive, true negative, false positive and false negative. Segmenting object pixel as a background is considered a FP, and segmenting background pixel as an object is considered a FN.  $TP$  and  $TN$  are the cases where an object is segmented as an object and a background is segmented as a background, respectively. Table 1 shows the comparison of segmentation performance for possible values of the three parameters  $\alpha$ ,  $\beta$  and  $\gamma$  in the three synthetic images, i.e., texture, blurred, and noisy image.

As expected we can observe that the robust alignment term is tuned to play the dominant role in the segmentation of the texture image as shown in Table 1. The alignment term in the speed function has a greater influence than the other terms on segmentation of the texture image. How-

**Table 2** ACC value using three parameters for noisy image.

$\alpha \backslash \beta$	0.1	0.2	0.3	0.4	0.5	0.6	0.7	0.8
0.1				0.978	0.981	0.980	0.980	0.978
0.2			0.984	0.986	0.985	0.983	0.981	
0.3		0.985	0.985	0.987	0.987	0.985		
0.4	0.987	0.985	0.985	0.983	0.984			$\gamma=0.1$
0.5	0.987	0.986	0.983	0.983				$\gamma=0.2$
0.6	0.986	0.984	0.982					$\gamma=0.3$
0.7	0.984	0.982						$\gamma=0.4$
0.8	0.982							$\gamma=0.5$

**Table 3** ACC value using three parameters for blurred image.

$\alpha \backslash \beta$	0.1	0.2	0.3	0.4	0.5	0.6	0.7	0.8
0.1				0.842	0.897	0.877	0.964	0.967
0.2			0.937	0.970	0.960	0.967	0.967	
0.3		0.895	0.893	0.940	0.951	0.953		
0.4	0.870	0.878	0.870	0.858	0.933			$\gamma=0.1$
0.5	0.880	0.875	0.866	0.830				$\gamma=0.2$
0.6	0.879	0.862	0.829					$\gamma=0.3$
0.7	0.854	0.816						$\gamma=0.4$
0.8	0.818							$\gamma=0.5$

ever, the active region term has little contribution to exact segmentation. Table 2 presents that the smoothing term is the important factor while the robust alignment term and the active region term both make little contribution to good segmentation for noisy image. Finally, we can observe that the active region term has the dominant contribution to the blurred image as shown in Table 3, but neither the robust alignment term nor the smoothing term contribute to good segmentation.

#### 4.2 Segmentation Results Based on the Proposed Method

In the second experiment, we also compared the performance of traditional approaches and the proposed approach for object segmentation in synthetic images with noise and blurring. Here the blurred image is obtained by applying a Gaussian blurring with radius 1.5 pixel on the original synthetic image. We have generated the noisy image by adding the Gaussian noise to the original image. The test synthetic image contained objects of different shapes, locations, sizes, and intensities. The traditional approaches are threshold-based speed function [19], Bhattacharyya-based speed function [18], [22], edge-based speed function [11], Georgiou-based speed function [20], mean-based speed function [12], and mean variance-based speed function [21]. In the experiment, we applied to the noisy and blurred versions of the synthetic image and results after 900 iterations are shown in Figs. 5 and 6. As it can be observed, the proposed approach is efficient for segmenting the objects.

As final experiment, the performance of the above-mentioned deformable models was tested and analyzed by using several types with a tumor region in magnetic resonance (MR) image of  $256 \times 256$  size. A MR scanner using a standard clinical imaging protocol was used to obtain the sample T1-weighted (T1) and contrast-enhanced T1 images. These MR images included concave tumors; there were also convex tumors with weak edges. The MR brain images without noise were used to identify the method that could segment a tumor region reflecting diverse contrast within the

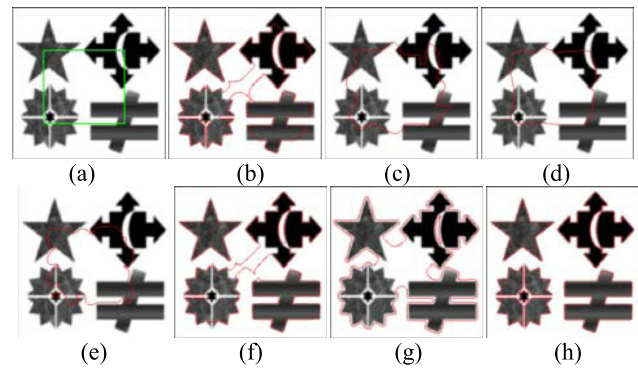


**Fig. 5** The segmentation results of objects on blurred image: (a) the contour position for the original image, (b) the result of the threshold-based speed function, (c) the result of the Bhattacharyya-based speed function, (d) the result of the edge-based speed function, (e) the result of Georgiou-based speed function, (f) the result of the mean-based speed function, (g) the result of the mean-variance-based speed function, (h) the result of the proposed approach ( $\alpha = 0.2, \beta = 0.5, \gamma = 0.3$ ).

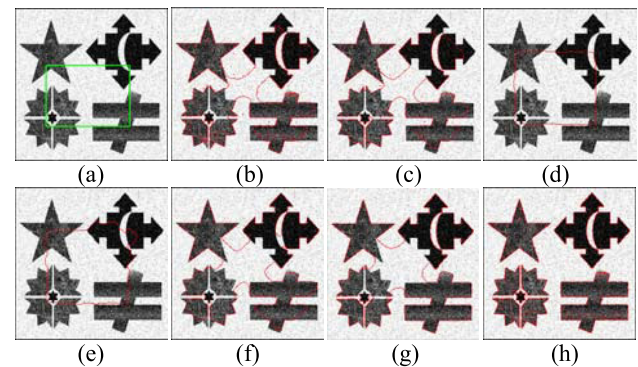


**Fig. 6** The segmentation results of objects on noisy image: (a) the contour position for the original image, (b) the result of the threshold-based speed function, (c) the result of the Bhattacharyya-based speed function, (d) the result of the edge-based speed function, (e) the result of Georgiou-based speed function, (f) the result of the mean-based speed function, (g) the result of the mean-variance-based speed function, (h) the result of the proposed approach ( $\alpha = 0.2, \beta = 0.2, \gamma = 0.6$ ).

target boundary.

Initialization for segmentation is done in the tumor region. Figures 7(a) and 8(a) show initialized curves for convex and concave tumor. The results are segmented a tumor region after 500 iterations. Figure 7 shows the tumor segmentation results of the hybrid speed function based on boundary and region information. The test image in Fig. 7(a) shows the initial curve overlapped with the original image. As shown in Figs. 7(b), (c), (d), (e), (f) and (g), the traditional approaches had almost the same result because there was no contour topology change. In particular, as shown in Figs. 7(c), (d) and (e), the tumor was under-segmented in the boundary region. In comparison, as shown in Fig. 7(h), the proposed approach accurately segmented images without resulting in isolated regions. Figure 8 shows the final segmentation results on a brain tumor image with an edema region. Figure 8(a) shows the initial curve overlapped with the original image. As shown in Figs. 8(b), (c),

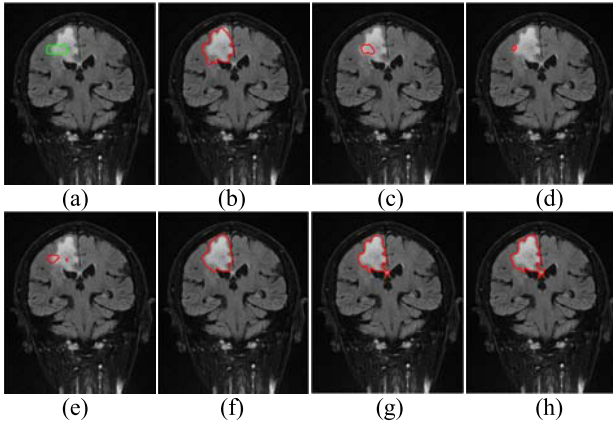


**Fig. 7** Final segmentation results for an MR brain image indicating a tumor: (a) the contour position for the original image, (b) the result of the threshold-based speed function, (c) the result of the Bhattacharyya-based speed function, (d) the result of the edge-based speed function, (e) the result of Georgiou-based speed function, (f) the result of the mean-based speed function, (g) the result of the mean-variance-based speed function, (h) the result of the proposed approach ( $\alpha = 0.3, \beta = 0.6, \gamma = 0.1$ ).

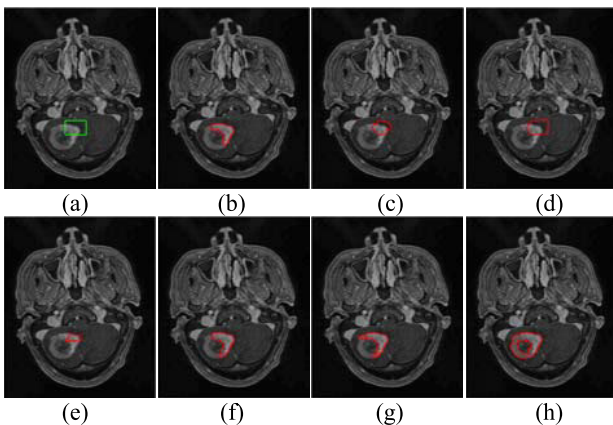


**Fig. 8** Final segmentation results for a brain tumor with edema region: (a) the contour position for the original image, (b) the result of the threshold-based speed function, (c) the result of the Bhattacharyya-based speed function, (d) the result of the edge-based speed function, (e) the result of Georgiou-based speed function, (f) the result of the mean-based speed function, (g) the result of the mean-variance-based speed function, (h) the result of the proposed approach ( $\alpha = 0.2, \beta = 0.7, \gamma = 0.1$ ).

(d), (e), (f), and (g), the tumor and edema regions were not segmented as two regions. Actually, the intensity in the tumor region was separated as two components as shown in Fig. 8 (h); the edema region was accurately segmented. As shown in Fig. 8 (h), the proposed approach accurately segmented the test images.

The proposed method accurately segmented the object region. As these results suggest, the proposed method can segment a variety of tumors as long as there is a sufficient intensity difference between the tumor and non-tumor regions in a given image.

Finally, we tested the effectiveness of the proposed method by using a natural (horse) image as shown in Fig. 9. The image was then segmented. Figure 9 shows the segmentation results of the proposed method and others. The

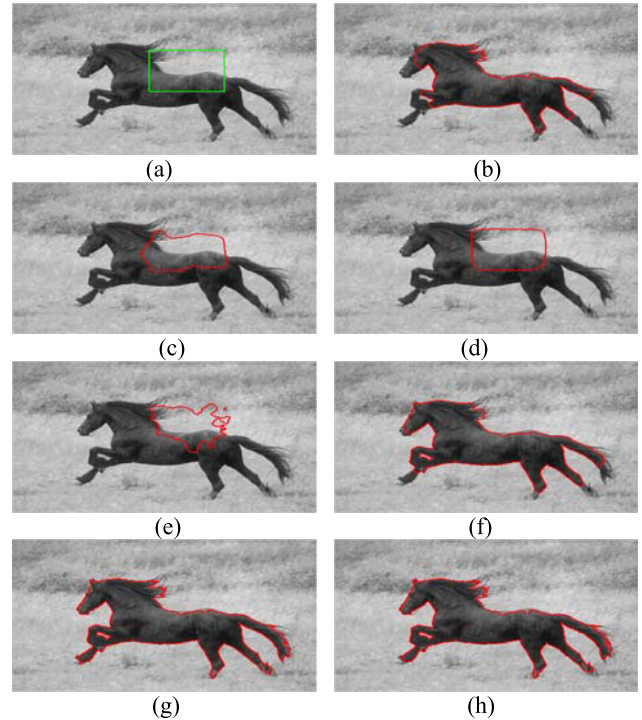


**Fig. 9** Result for the segmented horse region in a nature scene image: (a) the original image and the initial curve, (b) the result of the threshold-based speed function, (c) the result of the Bhattacharyya-based speed function, (d) the result of the edge-based speed function, (e) the result of Georgiou-based speed function, (f) the result of the mean-based speed function, (g) the result of the mean-variance-based speed function, (h) the result of the proposed approach ( $\alpha = 0.35, \beta = 0.35, \gamma = 0.3$ ).

boundary region between the object and the background was not accurately segmented. The result of the segmentation using the proposed approach is shown in Fig. 9 (h). Actually, we can observe that the segmentation result using natural scene is the same as shown in Figs. 9 (g) and (h).

## 5. Conclusions

This paper describes a novel hybrid speed function based on boundary and region information. The paper contributes by defining a new speed function based on the statistical information of the boundary and region of objects in an image. First, we use an external force for the active diffusion of gradient vectors of a gray-level edge map derived from the target image. Then, to compute region information, we adopt the Gaussian distributions to model the intensity distribution of the inside and outside of the evolving curve partitioning the image domain. We performed several experiments on a wide variety of MR images with a tumor region and compared the results of the proposed method with those of the traditional speed functions. The experimental results indicate that the proposed method can be effective in segmenting MR tumor images with poor contrast.

## Acknowledgement

This work was partially supported by two National Re-

search Foundations of Korea (NRF) grant funded by the Korean Government (MEST) (2010-0003360) and (KRF-2010-0013757).

## References

- [1] K.S. Fu and J.K. Mui, "A survey on image segmentation," *Pattern Recognit.*, vol.13, no.1, pp.3–16, 1981.
- [2] C. Li, C.Y. Kao, J.C. Gore, and Z. Ding, "Minimization of region-scalable fitting energy for image segmentation," *IEEE Trans. Image Process.*, vol.17, no.10, pp.1940–1949, 2008.
- [3] N. Paragios and R. Deriche, "Geodesic active regions and level set methods for supervised texture segmentation," *Int. J. Comput. Vis.*, vol.46, pp.223–247, 2002.
- [4] E.S. Gopi, *Algorithm collections for digital signal processing applications using Matlab*, Springer 2007.
- [5] T.S. Yoo, *Insight into images: Principles and Practice for Segmentation, Registration, and Image Analysis*, A K Peters, Ltd., Massachusetts 2004.
- [6] D. Jayadevappa, S.S. Kumar, and D.S. Murty, "A new deformable model based on level sets for medical image segmentation," *IAENG International Journal of Computer Science*, vol.36, no.3, pp.1–9, 2009.
- [7] R. Kimmel, "Fast edge integration," in *Geometric Level Set Methods in Imaging, Vision, and Graphics*, Springer, pp.59–79, 2006.
- [8] R. Goldenberg, R. Kimmel, E. Rivlin, and M. Rudzsky, "Cortex segmentation: A fast variational geometric approach," *IEEE Trans. Medical Imaging*, vol.21, no.2, pp.1544–1551, 2002.
- [9] M. Kass, A. Witkin, and D. Terzopoulos, "Snakes: Active contour models," *Int. J. Comput. Vis.*, vol.1, pp.321–331, 1988.
- [10] M. Leventon, W. Grimson, and O. Faugeras, "Statistical shape influence in geodesic active contours," *Proc. IEEE Conference Computer Vision and Pattern Recognition, I*, pp.316–323, 2000.
- [11] V. Caselles, R. Kimmel, and G. Sapiro, "Geodesic active contours," *Int. J. Comput. Vis.*, vol.22, no.1, pp.61–79, 1997.
- [12] T.F. Chan and L.A. Vese, "Active contours without edges," *IEEE Trans. Image Process.*, vol.10, no.2, pp.266–277, 2001.
- [13] N. Paragios and R. Deriche, "Geodesic active regions for texture segmentation," *Technical Report 3440, INRIA, France*, 1998.
- [14] C. Li, L. Wang, C. Kao, Z. Ding, and J. Gore, "Brain MR image segmentation by minimizing scalable neighborhood intensity fitting energy: A multiphase level set approach," presented at the ISMRM (2008).
- [15] S. Osher and J.A. Sethian, "Fronts propagating with curvature dependent speed: Algorithms based on Hamilton-Jacobi formulations," *J. Computer Physics*, vol.79, no.1, pp.66–71, 1997.
- [16] C. Xu and J.L. Prince, "Snakes, shapes, and gradient vector flow," *IEEE Trans. Image Process.*, vol.7, no.3, pp.359–369, 1998.
- [17] Y. Zhang, B.J. Matuszewski, L.K. Shark, and C.J. More, "Medical image segmentation using new hybrid level set method," *International Conference Biomedical Visualization*, 2008.
- [18] O. Michailovich, Y. Rathi, and A. Tannenbaum, "Image segmentation using active contours driven by the Bhattacharyya gradient flow," *IEEE Trans. Image Process.*, vol.16, no.11, pp.2787–2801, 2007.
- [19] S. Dambreville, A. Tannenbaum, A. Yezzi, and M. Niethammer, "A variational framework combining level-set and thresholding," *British Machine Vision Conference*, 2007.
- [20] R. Sandhu, T. Georgiou, and A. Tannenbaum, "A new distribution metric for image segmentation," *SPIE Medical Imaging*, vol.6914, pp.691404.1–691404.9, 2008.
- [21] M. Rousson and R. Deriche, "A variational framework for active and adaptive segmentation of vector valued images," *IEEE Workshop on Motion and Video Computing*, pp.1–18, 2002.
- [22] Y. Rathi, O. Michailovich, J. Malcom, and A. Tannenbaum, "Seeing the unseen: Segmenting with distributions," *International Conf. of Signal and Image Processing*, pp.1–5, 2006.
- [23] G. Kuhne, J. Weickert, M. Beier, and W. Effelsberg, "Fast implicit active contour models," *Lect. Notes Comput. Sci.*, vol.2449, pp.133–140, 2002.
- [24] R. Malladi, J.A. Sethian, and B.C. Vemuri, "Shape modeling with front propagation: A level set approach," *IEEE Trans. Pattern Anal. Mach. Intell.*, vol.17, no.2, pp.158–175, 1995.
- [25] W. Cho, J. Park, S. Park, S. Kim, S. Kim, G. Ahn, M. Lee, and G. Lee, "Level-set segmentation of brain tumors using a new hybrid speed function," *International Conference on Pattern Recognition*, pp.1545–1548, 2010.
- [26] P.Y. Chou and G.D. Fasman, "Prediction of the secondary structure of proteins from their amino acid sequence," *Adv. Enzymol. Relat. Areas Mol. Biol.*, vol.47, pp.45–148, 1978.



**Jonghyun Park** received the M.S. and Ph.D. degrees in electronics engineering from Mokpo National University, Korea, in 1997 and 2001, respectively. He researched as a Postdoctoral fellowship in computer science from Chonbuk National University from 2003 to 2004. He was a visiting scholar in Computer Science from University of Southern California (USC), Los Angeles, California, from 2004 to 2006. He was a research professor of Chonnam National University, Korea, from 2006 to 2010. He is currently an industry-university cooperation oriented professor, Mokpo National University. His research interests include low to mid-level visions such as condition monitoring system, segmentation, shape analysis, pattern recognition, medical image processing and computer vision topics.



**Soonyoung Park** received B.S. degree in electronics engineering from Yonsei University, Seoul, Korea in 1982 and M.S. and Ph.D. degrees in electrical and computer engineering from State University of New York at Buffalo, in 1986 and 1989, respectively. From 1989 to 1990 he was a Postdoctoral Research Fellow in the department of Electrical and Computer Engineering at the State University of New York at Buffalo. Since 1990, he has been a Professor with Department of Electronics Engineering, Mokpo National University, Korea. His research interests include biomedical image processing, image retrieval techniques, and monitoring technique for wind energy systems.



**Wanhyun Cho** received the B.S. and M.S. degrees in Mathematics from Chonnam National University in 1977 and 1981, and Ph.D. degree in Statistics from Korea University in 1988, respectively. Since 1983, he has been Professor with Department of Statistics in Chonnam National University, Korea. His research interests include Pattern recognition, Medical image processing, Image matching and retrieval techniques, and HDP-2DHMM.